Exploitation of Luminescent Lanthanide Nanoparticles for a Sensitivity-Enhanced ELISA Detection Method

Ali Kassir, Clémence Cheignon, Loïc Charbonnière

Exploitation of luminescent lanthanide nanoparticles for a sensitivity-enhanced ELISA detection method

Ali A. Kassir,† Clémence Cheignon, Loïc J. Charbonnière*

Equipe de Synthèse pour l'Analyse, IPHC, UMR 7178 CNRS, Université de Strasbourg, ECPM, 67087 Strasbourg, France

ABSTRACT: A new detection method based on the photoluminescence properties of dye-sensitized lanthanide nanoparticles (Ln NPs) was developed for Enzyme Linked Immunosorbent Assays (ELISA). In this method, the Horseradish Peroxidase (HRP) enzyme catalyzes the oxidation of phenol derivatives in presence of hydrogen peroxide, providing dimers that are able to interact with the Ln NP surface and to efficiently photosensitize the Ln ions. Due to the very long emission lifetime of Ln, the time-gated detection of Ln NP luminescence allows elimination of background noise due to the biological environment. After a comparison of the enzyme catalyzed oxidation of various phenol derivatives, methyl 4-hydroxyphenyl acetate (MHPA) was selected as the most promising substrate as the highest Ln emission intensity was observed following its HRP catalyzed oxidation. After a meticulous optimization of the conditions of both the enzymatic reaction and the Ln sensitization (buffer, pH, concentration of the reactants, NP type …), this new detection method was successfully implemented in a commercial insulin ELISA kit as a proof-of-concept, with an increased sensitivity compared to the commercial detection method.

INTRODUCTION

Lanthanide compounds display unique highly useful optical properties and are widely used in several applications such as in lighting,[1] light conversion,[2] sensing,[3] bio-labeling[4] and bio-imaging.[5] The optical properties of Ln^{3+} ions arise from the electronic transitions within the 4f orbitals. These core orbitals are shielded and have little interaction with the chemical environment of the ion. Therefore, the f-f transitions display sharp and specific emission signatures for each lanthanide. These transitions are forbidden by the Laporte and sometimes spin multiplicity rules. This can be relaxed by symmetry considerations, resulting in very long excited-state lifetimes, which leads to almost background-free detection using time-resolved methods. However, the associated very weak absorptivity makes the direct excitation inefficient. Fortunately, this can be overcome with an indirect sensitization of Ln ions by a light-harvesting chromophore, a phenomenon called antenna effect.[6]

In the last decade, Ln^{3+} doped nanomaterials have emerged as excellent alternatives to Ln complexes.[7] In addition to the stability and the versatility, lanthanide nanoparticles (Ln NPs) provide better protection of Ln^{3+} ions from nonradiative deactivation *via* vibrational modes of the solvent or ligand framework, - with a concomitant enhancement of their luminescence properties (e.g. lifetime, brightness).[8] Globally, Ln NPs have found a growing interest in their study, development, and employment in multiple applications especially in bioanalytical fields such as bio-imaging, drug delivery, photodynamic therapy, and bioassays.[9]

Time resolved luminescence detection of lanthanides has been widely used to improve the sensitivity of immunoassays.[10,11] Different studies have attempted to combine this technique with an enzymatic amplification in a highly promising approach called enzyme-amplified lanthanide luminescence (EALL). This consists of an enzyme-catalyzed formation of a ligand, which, in contrast to the substrate, is able to chelate and photosensitize Ln^{3+} ions. The luminescence of the formed complex is selectively measured by time-resolved detection. This strategy can be used to simply detect enzymatic conversion, but also to detect immunogenic reactions between an antibody and its antigen (Ab-Ag) in assays where the enzyme is used as a label, as in ELISA.[12–14]

Most developed EALL methods have been performed at alkaline pH, to allow the coordination of the ligand to the lanthanide. However, at high pH, it is required to add ethylenediaminetetraacetic acid (EDTA) chelate to avoid the formation of insoluble lanthanide hydroxide, resulting in ternary complexes in solution. The use of EDTA is also mandatory to fulfill the coordination sphere of the Ln atoms, repelling the solvent molecules from the first coordination sphere. This thereby decreases the deleterious impact of these molecules on the luminescence efficiency of the Ln atoms.[15,16] However, the use of EDTA is unfavorable in terms of sensitivity because the EDTA itself can sensitize Ln^{3+} to a small extent, contributing to the background signal, while excess of EDTA also reduces the efficiency of the sensitization by the antenna. These drawbacks have thus far limited their development and commercialization.

Herein, we propose a new sensitive ELISA detection method based on luminescent lanthanide nanoparticles (Scheme 1). As Ln atoms are embedded in the NP structure, the surface Ln ions' coordination sphere is already partly satisfied bt NP subsurface Ln-F bonds, leaving only two to three coordination sites vacant for the coordination of antennae at the surface of the NPs.[17] Ln NPs can overcome the limitations of Ln-complexes by providing better stability at larger range of pH and can also add further improvement in brightness and lifetime.

In this work, we have prepared and characterized two sets of LaF_3 based NPs with different doping Ln atoms (Tb-Eu) and

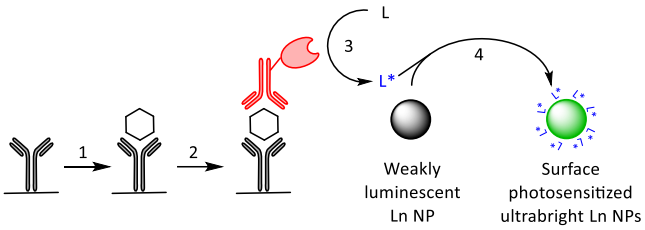

Scheme 1: Principle of the new detection method based on Ln NPs for ELISA. 1) fixation of the analyte on a surface immobilized primary antibody. 2) fixation of an enzyme-functionalized secondary antibody. 3) Enzymatic reaction of the substrate resulting in the formation of photosensitizers L^*. 4) binding of L^* at the surface of the NPs to amplify their luminescence by antenna effect.

ratios. Then we have designed and optimized an enzymatic reaction (Scheme 1, step 3) to convert an inactive substrate (L) into a ligand (L^*) able to coordinate to the Ln NPs surface and to photosensitize Ln ions (Scheme 1, step 4). Finally, the developed method has been implemented in an ELISA system for the detection and quantification of human insulin (Scheme 1, all steps) and compared to the state-of-the-art conventional colorimetric detection method.

EXPERIMENTAL SECTION

Materials and Reagents. High purity Ln salts ($LaCl_3.7H_2O$, $TbCl_3.6H_2O$ and $EuCl_3.6H_2O$), ammonium fluoride, Horseradish peroxidase (HRP) powder (type VI, 250 Units/mg), Bovine liver Catalase powder (2000-5000 Units/mg), Streptavidin-HRP (SA-HRP) conjugate (1 mg in 0.05 mol·L^{-1} HEPES pH 6.8), Hydrogen peroxide 30%, succinic acid 99%, and MQuant® semi quantitative colorimetric peroxide test strips, were purchased from Sigma. Methyl 4-hydroxyphenylacetate 97% was purchased from Fluorochem. The other used phenols were purchased from Sigma, Fluorochem or TCI chemicals. Human insulin ELISA kit (EZHI-14K) was purchased from Merck Millipore.

Synthesis and characterization of Ln-doped nanoparticles. $La_{0.9}Tb_{0.1}F_3$ and $Tb_{0.85}La_{0.14}Eu_{0.01}F_3$ NPs were prepared in aqueous solution using a microwave oven, according to the previously published procedure[18] described for $La_{0.9}Tb_{0.1}F_3$ NPs and adapted for $Tb_{0.85}La_{0.14}Eu_{0.01}F_3$ NPs (see SI for detailed preparation procedure). Their shape and composition were characterized by TEM, zeta potential measurement, DLS and ICP-AES analysis. TEM measurements were performed with a JEOL 2100F electron microscope operating at 200kV equipped with a GATAN GIF 200 electron imaging filter, coupled with energy dispersive X-ray (EDX) spectroscopy, with a point-to-point resolution of 0.23 nm. A drop of the suspension of nanoparticles in water was deposited on TEM grids. The grid was prepared with a porous membrane covered by an amorphous carbon layer. The zeta potential and the hydrodynamic diameter were measured using an AMERIGO system (Cordouan technologies). All measurements were done in milliQ water at room temperature. DLS measurements were performed using an external probe with laser at 638 nm. The experimental correlograms are fitted by SBL mathematical algorithm and the results were treated by the number of NPs. Laser Doppler electrophoresis measurements were performed in solutions diluted 50 times from stock solution at 20.27 V·cm^{-1} applied electric field. Zeta potential is directly linked to the mobility of NPs according to the theory of Smoluchovski. Results are given as the mean value of at least 6 experiments with their standard deviations. ICP-AES analyses were performed with a Varian 720-ES spectrometer equipped with a quartz Meinhard nebulizer and a cyclone spray chamber. The concentration was determined by comparison with commercial standard samples.

The stability of the stock solution of NPs was verified over four months by controlling that the size (hydrodynamic diameter measured by DLS), charge (zeta potential) and pH of the stock solution remain constant.

Spectroscopic measurements. Steady-state fluorescence measurements of the ligands, time-resolved photoluminescence measurements of Ln NPs, and absorbance measurements of TMB were all recorded on a TECAN Spark multimode microplate reader with monochromators, working with a high energy Xenon flash lamp, in low-binding black 96-wells microplates from Greiner Bio-one. Time-resolved measurements were recorded with a time delay of 50 µs and an integration time of 2 ms.

Enzymatic assays. All enzymatic assays were performed in a total volume of 200 µL (the following concentrations are given for this solution volume) in low-binding black 96-wells microplates from Greiner Bio-one. 2 mmol·L^{-1} of the *p*-substituted phenol and 0.2 mmol·L^{-1} of H_2O_2 were incubated in microplate wells in 10 mmol·L^{-1} succinate buffer at pH 4.6 (HRP) or pH 7.0 (SA-HRP). The reaction was normally initiated by the addition of HRP enzyme and the microplate was agitated in a microplate shaker (400 rpm) at room temperature for 1 h. Concentrations and pH conditions can vary in the optimization procedure of each parameter. For kinetics studies, the microplate was agitated in the TECAN incubator and the increase in fluorescence (λ_{exc} = 289 nm, λ_{em} = 402 nm), was recorded for 1 h of reaction. 0.05 mg·mL^{-1} of catalase (5 µL of a 2 mg·mL^{-1} solution) were introduced to the mixture, and the elimination of H_2O_2 was verified by colorimetric peroxide test strips before the addition of the NPs. Finally, 2×10^{-8} mol·L^{-1} of Ln NPs were added to the reaction mixture, the pH was increased to *ca* 13 using 8 µL of a 1 mol·L^{-1} NaOH solution and the microplate was agitated for 5 min. The excitation spectra were recorded at an emission of 545 nm of Tb, while the emission spectra were recorded at the maximal excitation. The excitation and emission bandwidths, the gain, as well as the z-position were kept constant in order to compare the different datasets. All experiments were repeated at least three times with no significant variation.

HPLC-UV analysis. Samples of the reaction mixture in presence and in absence of HRP as well as the reference compounds were analyzed by HPLC-UV (Agilent technologies Series 1100 system equipped with a quaternary pump), separated on a C18-AQ Interchim puriFlash column (4.6 × 250 mm, 5µm) with an injection volume of 10 µL. The gradient elution was carried out with ultrapure water and acetonitrile (ACN) at a flow rate of 1.0 mL.min^{-1}. The mobile phase gradient was programmed with the following time course: 50% ACN at 0 min, linear increase to 100% ACN at 8 min, linear decrease to 50% ACN at 10 min and held 5 min. The absorption of the eluted compounds was detected at λ_{abs} = 220 nm.

LOD/LOQ calculation. Limit of detection (LOD) and limit of quantification (LOQ) were estimated by measuring replicates of blank sample, determining the mean value and the standard deviation (SD), and calculating LOD as the mean plus 3.3 SD and the LOQ as the mean plus 10 SD. The coefficients 3.3 and 10 are obtained assuming a 95% confidence level.

ELISA procedure. The ELISA procedure was realized according to the protocol of the commercial kit "Human insulin ELISA kit (EZHI-14K)" (Merck Millipore). The classical procedure was fully followed for the detection with TMB, however some changes have been operated for the implementation of the detection method with Ln NPs. After the incubation with the enzyme conjugate solution followed by the washing steps, 2 mmol·L^{-1} of methyl 4-hydroxyphenyl acetate (MHPA) and 0.2 mmol·L^{-1} of H_2O_2 were incubated in microplate wells in 10 mmol·L^{-1} succinate buffer pH 7.0. The final volume in the wells was fixed at 200 µL in all assays. The microplate was agitated in a microplate shaker (400 rpm) at room temperature for 1 h. 0.05 mg·mL^{-1} of catalase were introduced to the mixture, prior to the addition of 2 × 10^{-8} mol·L^{-1} of $Tb_{0.85}La_{0.14}Eu_{0.01}F_3$ NPs to the reaction mixture, and the pH increase to approximately 13 by addition of 8 µL of a 1 mol·L^{-1} NaOH solution. The microplate was then agitated for 5 min and the time-resolved emission was measured at 545 ± 3.5 nm after excitation at 318 ± 5 nm with a lag time of 50 µs and an integration time of 2.0 ms.

RESULTS AND DISCUSSION

Lanthanide nanoparticles synthesis

$La_{0.9}Tb_{0.1}F_3$ and $Tb_{0.85}La_{0.14}Eu_{0.01}F_3$ nanoparticles (NPs) were prepared in aqueous solution using a microwave oven, according to the previously published procedures.[18,19] These two types of Tb doped and Tb/Eu doped LaF_3 NPs were chosen for their morphological and spectroscopic differences and will be tested to identify the most suitable for the developed detection method. Transmission electron microscopy (TEM) images (Figure 1a-b) indicate the presence of rounded or slightly elongated shaped NPs (especially in the case of $Tb_{0.85}La_{0.14}Eu_{0.01}F_3$) with an average diameter of 20 ± 6 and 35 ± 7 nm for $La_{0.9}Tb_{0.1}F_3$ and $Tb_{0.85}La_{0.14}Eu_{0.01}F_3$ NPs respectively, with a controlled dispersity (Figure 1c). Zeta potential measurements in aqueous solution show that both NPs exhibit a positive surface charge superior to + 30 mV (Figure 1d), highlighting a good colloidal stability with limited aggregation, supported by the DLS measurements which reveal well dispersed NPs with mean hydrodynamic diameters of 49 ± 14 nm and 62 ± 18 nm for $La_{0.9}Tb_{0.1}F_3$ and $Tb_{0.85}La_{0.14}Eu_{0.01}F_3$ NPs respectively (Figure 1d and Figure S1). Both TEM and DLS results indicate that the Tb/Eu doped NPs are bigger than the Tb doped NPs, probably originating from the different crystal structure ($La_{0.9}Tb_{0.1}F_3$ exhibiting a hexagonal LaF_3 as previously reported[18] while $Tb_{0.85}La_{0.14}Eu_{0.01}F_3$ related XRD structure corresponds to an orthorhombic TbF_3 crystal structure as shown in Figure S3).

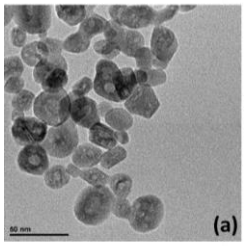

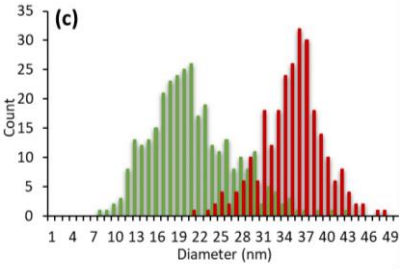

(d)	$La_{0.9}Tb_{0.1}F_3$	$Tb_{0.85}La_{0.14}Eu_{0.01}F_3$
Diameter (nm)*	20 ± 6	35 ± 7
Zeta potential (mV)	37 ± 8	35 ± 5
Hydrodynamic diameter (nm)	49 ± 14	62 ± 18 nm

Figure 1: Transmission electron microscopy images of (a) $La_{0.9}Tb_{0.1}F_3$ and (b) $Tb_{0.85}La_{0.14}Eu_{0.01}F_3$ NPs; (c) Particle size distribution *of* $La_{0.9}Tb_{0.1}F_3$ (green) and $Tb_{0.85}La_{0.14}Eu_{0.01}F_3$ (red) NPs determined by TEM and (d) summary table with the mean diameter determined by TEM(*), zeta potential (calculated from mobility measurements shown in Figure S2) and mean hydrodynamic diameter determined by DLS for each type of NPs (DLS graph with size distribution shown in Figure S1).

The NPs composition was characterized by inductively coupled plasma atomic emission spectroscopy (ICP-AES) analysis and their concentration was determined following the previously published method,[18] by using the average diameter of the NPs determined by TEM measurement, the density of $La_{0.9}Tb_{0.1}F_3$ and $Tb_{0.85}La_{0.14}Eu_{0.01}F_3$ calculated as the percentage weighted density of LaF_3, TbF_3 and EuF_3 (for the last NPs), and the total amount of La (or Tb or Eu) in the solution, as determined by ICP-AES analysis (Table S1).

Enzymatic dimerization of phenol derivatives

12 para-substituted phenol derivatives (Figure 2) were selected as substrates for the HRP catalyzed dimerization reaction followed by testing a potential photosensitization of Tb in the NPs (Scheme 2). For the development of this method, several parameters have to be considered: the enzymatic reaction yield leading to the desired product and the capacity of both the substrate and the dimer product(s) to sensitize the Tb of the NPs.

As a prerequisite, all the selected substrates were demonstrated to be very poor photosensitizing ligands, as some phenol containing compounds such as calix[4]arenes, have been shown to photosensitize Tb in NPs.[20] For this purpose, each ligand was added to a solution of NPs and after increasing the pH to 13 (see procedure below) the very low Tb emission was measured after excitation at the wavelength selected for Tb sensitization by the reaction product (Figure S4). Para- substituted compounds were chosen as it can (i) help to promote the formation of the *o,o*'-biphenol, the best candidate for Ln coordination among the various potential dimeric products,[21] (ii) influence the solubility of the formed dimer in water and (iii) directly affect the pKa of the phenol group,[22] and (iv) impact the fluorescence capacity of the oxidation product as well as its ability to sensitize specific Ln ions.[23] Finally, the application of an alkaline pH is mandatory for the detection step in order to deprotonate the phenol moieties, and thus obtain a stronger coordination and a more efficient Ln photosensitization.

For each substrate, in a total volume of 200 µL, 1 mmol·L^{-1} were incubated in microplate wells with H_2O_2 0.5 mmol·L^{-1} at pH 7.0, and the reaction was initiated by the addition of HRP

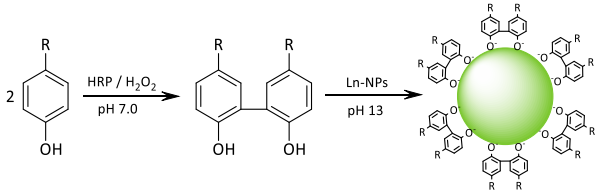

Scheme 2: Representation of the two distinct steps of the developed method: HRP catalyzed dimerization of *p*-substituted phenol derivatives leading to the desired *o,o'*-biphenol product followed by the Tb photosensitization by the biphenolate product present at the surface of the NPs at alkaline pH.

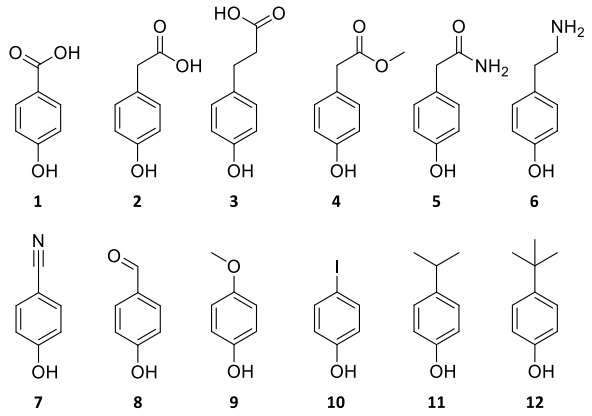

Figure 2: Substrates with different *p*-substituents tested in the assay.

enzyme (10^{-9} mol·L^{-1}). After one hour of reaction, catalase was added to the mixture to neutralize the remaining H_2O_2, followed by the introduction of 2×10^{-8} mol·L^{-1} $La_{0.9}Tb_{0.1}F_3$ NPs and the pH was increased to 13. While the first pKa of o,o'-biphenol is found around 7.6, the second pKa value is around 13 [22] and the large increase of the pH of the solution ensures the second deprotonation and a better coordination at the surface of the NPs as shown in Figure S5. Finally, the Time Resolved (TR) emission spectra were measured with respect to the maximum excitation determined for an emission at 545 nm in each well. Figures 3a and 3b show the TR-emission spectra of Tb with the substrates presenting the most interesting results (See Supporting Information, Figure S6 for substrates 6 to 10 or in absence of substrate), and the turn-on amplification factor obtained with all tested substrates respectively.

The three substrates containing a carboxylic acid group (1, 2 and 3) were all found to sensitize Tb-NPs, substrates 2 and 3 exhibiting a much higher amplification of Tb emission than substrate 1 upon HRP catalyzed oxidation. These results are in accordance with the proposition of Guilbault *et al*, stating that a methylene group in *para* position yields to a better fluorescent dimer product,[24] and tend to highlight that the coordination of the corresponding biphenolate on the surface of the NPs occurs through the phenolic group. However, the potential (partial) involvement of the carboxylate groups in the coordination, as supported by Zheng *et al.* in a previous report,[25] cannot be discounted.

The methyl 4-hydroxyphenyl acetate (4) was tested as a protected version. The oxidation of this substrate provided the highest Tb emission amplification with a factor of 1220, a drastic enhancement compared with the substrates 1-3. It is assumed that the protection oftwo negatively charged carboxylate groups as methyl ester functions prevents the attraction to the NPs from this side and favors the coordination of the dimer through the phenolic groups. This also protects the reactive carboxylate from any side reaction, such as its oxidation to a carboxylic radical followed by addition to the *meso*-position.[26]

An analogous substrate (5) with an amide group was proposed to provide a higher stability than the ester group at alkaline pH. Unfortunately, the oxidation of this substrate did not offer the same Tb emission amplification and was limited to a factor of 660. As the fluorescent aromatic moiety of this substrate was not modified compared to substrate (4), a significant variation of the antenna triplet state is not expected. Therefore, this halving in the sensitization efficiency is not completely related to the spectroscopic properties of these antennae but may be due to the formation yield of each one of them following the enzymatic oxidation. The NH group of the amide acts as a hydrogen donor and can be more or less reactive to HRP oxidation, conducting to side products altering the formation yield of the sensitizer. This hypothesis was strengthened by the results obtained with substrate (6), containing an amine group. Despite that the obtained dimer has approximately the same spectroscopic properties as the carboxylic acid analogous,[23] no sensitization of Tb emission was observed. Substrates with electron-withdrawing (7,8) or donating (9,10) substituents did not lead to any photosensitization following the enzymatic reaction, probably due to an inhibition of the reaction, as the elimination of the methylene group in the side chain was demonstrated to decrease the rate of oxidation.[23] Another hypothesis is that electron-donating and withdrawing substituents by the mesomeric effect can modify the π-electrons delocalization of the aromatic moiety which significantly alters the triplet state of the formed dimer. This could either increase the energy gap with the Tb emissive state, inhibiting the transfer, or reduce this gap resulting in back transfer to the ligand. Finally, oxidation of substrates 11 and 12 with only carbon chain substituents shows very low signal amplification, most probably originating from solubility issues.

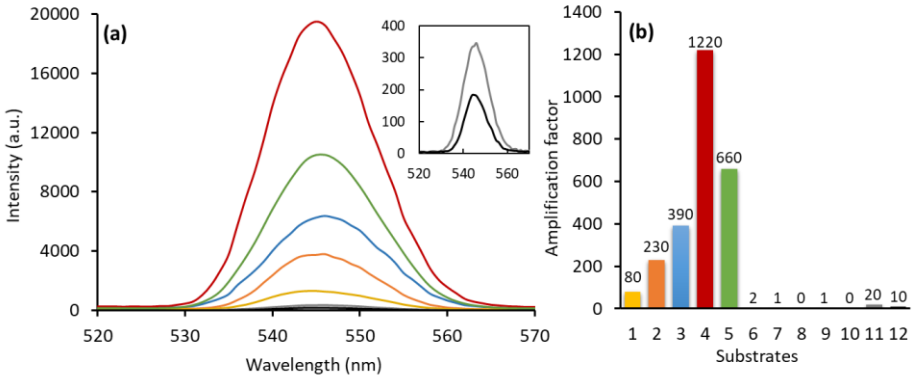

Figure 3: (a) TR-emission spectra of $La_{0.9}Tb_{0.1}F_3$ NPs (λ_{exc} = 320 nm) after HRP catalyzed oxidation of the most promising substrates (1: yellow, 2: orange, 3: blue, 4: red, 5: green. Inset: 11: grey, 12: black). (b) Amplification factor obtained with all tested substrates, calculated by dividing the substrate related intensity at 545 nm with one of the blank from Figure 3a and Figure S6. TRIS buffered solution (10 mmol·L^{-1}, pH 7.0) containing HRP (10^{-9} mol·L^{-1}), substrate (1 mmol·L^{-1}) and H_2O_2 (0.5 mmol·L^{-1}).

Characterization of HRP-catalyzed oxidation of MHPA

The methyl 4-hydroxyphenyl acetate (substrate 4, named MHPA) was selected as substrate for the next steps as it provided the best performance in this enzymatic assay. The reaction mixture was then analyzed after one hour by HPLC-UV (Figure 4 and Figure S7, blue trace). As a control, a reaction mixture with no HRP was also analyzed (black trace). A decrease of the peak with a retention time of 4.3 min, corresponding to the MHPA, is clearly observed, confirming the reaction in presence of both H_2O_2 and HRP. In the reaction mixture, two other peaks are observed at 5.3 and 5.9 min. In order to know if the desired *o,o'*-biphenol is formed during this reaction, the dimeric dimethyl-2,2'-(6,6'-dihydroxy-[1,1'-biphenyl]-3,3'-diyl)diacetate (named *o,o'*-biphenol) was synthesized from MHPA according to a described procedure *via* a biomimetic iron(III)-catalyzed solid-phase coupling reaction.[27] The resulting product has been characterized by ^{1}H NMR (see SI for assignment of NMR signals) and analyzed by HPLC-UV (Figure 4, red trace). The peak at 5.3 min in the reaction mixture can thus be assigned to the *o,o'*-biphenol as both the retention time and the UV absorbance spectra (Figure 4, inset) are comparable. The second peak has not been characterized but it is assumed that it is a product from the *o,o'*-biphenol, as an increase of the intensity of this peak along with a decrease of both the peaks at 4.3 and 5.3 min is observed after a second addition of H_2O_2 (see Figure S8).

The reaction mixture has also been characterized by fluorescence spectroscopy (Figure S9). The oxidation product is strongly fluorescent and presents excitation and emission maxima at 289 nm and 402 nm, respectively. In contrast, the starting MHPA substrate is weakly fluorescent under these conditions, thus fluorescence spectroscopy is a suitable tool to follow the reaction kinetics.

Optimization of the dimerization reaction of MHPA

The kinetics of HRP catalyzed MHPA oxidation was monitored by fluorescence spectroscopy, first of all under mild enzyme concentration (Figure 5, blue dots). The formation of the dimer was strictly dependent on the presence of HRP enzyme in the reaction mixture as no increase of intensity was observed if HRP was not added (Figure 5, grey dots).

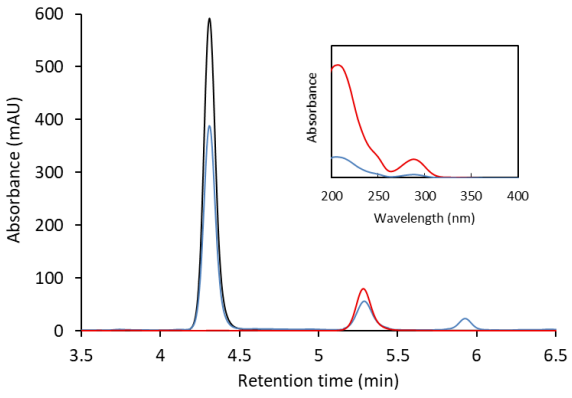

Figure 4: Enlargement of the chromatogram traces of the reaction mixture in presence (blue) and absence (black) of HRP and of the synthetic dimer (red) (λ_{abs} = 220 nm). The full chromatogram traces are shown in Figure S7. Inset: UV spectra of the synthetic dimer (red) and the enzymatic product (blue) at a retention time of 5.3 min (TRIS/HCl, 10 mmol·L^{-1}, pH 7.0, [MHPA] = 1 mmol·L^{-1}, [HRP] = 0 or 10^{-10} mol·L^{-1} and [H_2O_2] = 0.5 mmol·L^{-1}).

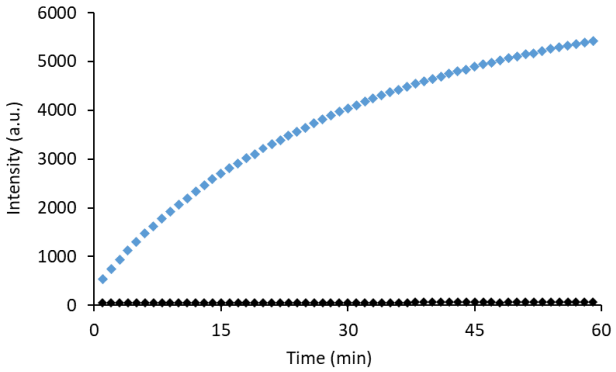

Figure 5: Kinetics of HRP catalyzed MHPA oxidation in presence of H_2O_2 monitored by fluorescence with HRP 10^{-10} mol·L^{-1} (blue dots) or without HRP black dots). (λ_{exc} = 289 nm, λ_{em} = 402 nm, TRIS/HCl, 10 mmol·L^{-1}, pH 7.0, [MHPA] = 1 mmol·L^{-1}, [HRP] = 0 or 10^{-10} mol·L^{-1} and [H_2O_2] = 0.5 mmol·L^{-1}).

Several parameters can influence the enzymatic reaction and the NP photosensitization, such as the pH and the concentration of the various reagents. The effect of the pH on the enzymatic reaction was studied in the pH range from 3.5 to 8.5 (Figure 6). The highest fluorescence intensity corresponding to the highest formation of the fluorescent dimer is observed for a pH of 4.6, far from the pH 7.0 already discussed (*vide supra*). This result is quite surprising as numerous HRP-catalyzed oxidation of phenols have been reported for pH between 6.5 and 8.5.[28] However, the amount and nature of the products have been shown to depend on the type of HRP,[29] and different properties can be obtained for various commercial preparations of HRP.[30] In addition, oxidation of several substrates by HRP was reported at acidic pH including guaiacol, 3,3′,5,5′-Tetramethylbenzidine (TMB) and others.[31]

The ratio of H_2O_2 to HRP has been found to be a crucial parameter for the phenol oxidation efficiency. While a lack of H_2O_2 during the reaction limits the reaction rate, an excess of H_2O_2 behaves as a typical suicide substrate of HRP enzyme.[32] In the presence of excess H_2O_2, other cycles of HRP can be triggered, where HRP is converted to a species (named compound III)[33] which slows down the peroxidase cycle responsible of phenol oxidation.[34] This phenomenon was investigated by monitoring the reaction kinetics at H_2O_2 concentrations in the range of 0.1-2 mmol·L^{-1}, while maintaining constant MHPA and HRP concentrations.

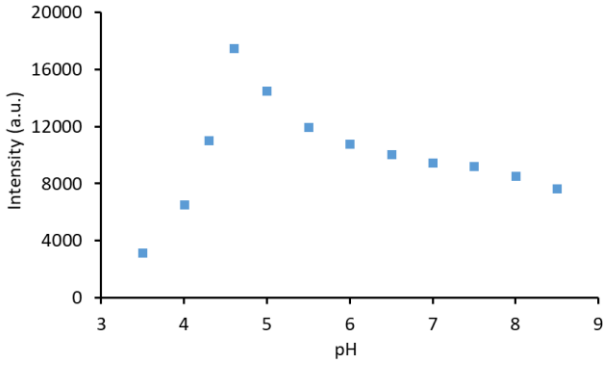

Figure 6: Effect of the pH on the formation of the MHPA dimer (λ_{exc} = 289 nm, λ_{em} = 402 nm). Fluorescence intensity measurement of a succinate buffered solution (10 mmol·L^{-1}) containing HRP (10^{-10} mol·L^{-1}), MHPA (2 mmol·L^{-1}) and H_2O_2 (0.5 mmol·L^{-1}).

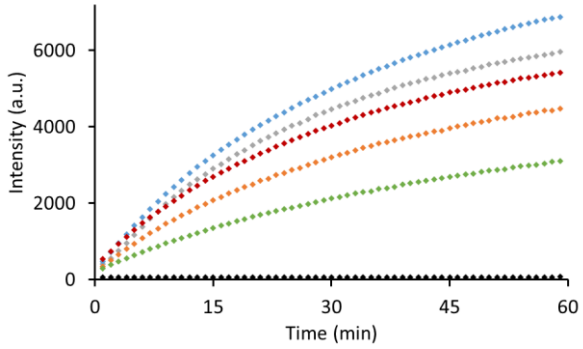

Figure 7: Kinetics of MHPA oxidation catalyzed by HRP with H_2O_2 concentrations of 0 (black), 0.1 (grey), 0.2 (blue), 0.5 (red), 1.0 (orange) or 2.0 mmol·L^{-1} (green). (λ_{exc} = 289 nm, λ_{em} = 402 nm, 10 mmol·L^{-1} succinate buffer, pH 4.6, [HRP] = 10^{-10} mol·L^{-1}, [MHPA] = 2 mmol·L^{-1} and H_2O_2).

As shown in Figure 7, in the range of 0.1-0.2 mmol·L^{-1}, the rate of the reaction increased with H_2O_2 concentration while for higher concentration (≥ 0.5 mmol·L^{-1}), the reaction rate diminished, highlighting the effect of excess H_2O_2 on the deactivation of the HRP enzyme. Thus, a HRP concentration of 0.2 mmol·L^{-1} appeared to be the best choice to obtain the highest quantity of dimer.

A similar experiment was realized by varying the substrate concentration (MHPA between 0.5 and 5 mmol·L^{-1}) in order to study its influence on both the enzymatic reaction (Figure S10, left panel) and the NP photosensitization (Figure S10, right panel). While the dimer fluorescence intensity continuously increases with the MHPA concentration (with a slight increase at higher concentrations compared to the lowest concentrations), the photoluminescence intensity of the NPs reaches the highest value for 2 mmol·L^{-1} before decreasing sharply for higher MHPA concentrations. This can be explained by a competition between the formed dimer and the remaining substrates to be coordinated at the surface of the NPs. For MHPA concentrations higher than 2 mmol·L^{-1}, the increase of dimer formed is less significant, but the quantity of initial substrate is much higher, thus the MHPA/dimer ratio strongly increases, and the formed dimer has less probability to be coordinated at the surface of the NP. After optimizing the conditions for an efficient formation of the antenna and maximal sensitization of $La_{0.9}Tb_{0.1}F_3$ NPs, the dependence of the final response on the enzyme concentration was investigated by establishing the corresponding calibration curve (Figure 8).

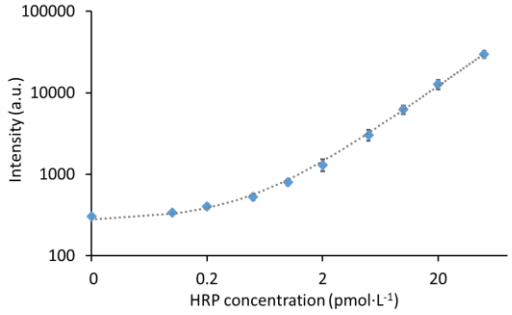

Figure 8: Calibration curve of the photoluminescence response of the assay as a function of HRP concentration (0.1 to 100 pmol·L^{-1}). Time-resolved emission measurement at 545 nm after excitation at 320 nm.

The developed method was tested on a large range of HRP concentrations between 0.1 and 100 pmol·L^{-1} under optimized conditions (pH 4.6, H_2O_2 and MHPA 0.2 and 2 mmol·L^{-1} respectively). The relative response of the assay as a function of the enzyme concentration fitted well in a linear equation (as illustrated by the linear regression shown in Figure S11 in a non-logarithmic scale) showing the expected linear behavior. The three replicates present low standard deviations which reflect the precision of the method. In addition, the dynamic range seems to be very important as the calibration curve covered three orders of magnitude and the upper limit of linearity of the method was not yet reached. Limits of detection (LOD) and of quantification (LOQ) of 0.1 and 0.3 pmol·L^{-1} were determined, respectively (see experimental section for more details), highlighting the sensitivity of the detection. As a comparison, this HRP detection method is 8000 and 20 times more sensitive than the best conditions of similar assays using Ln complexes.[25,35] Thus, according to the very encouraging results, this method can now be implemented in a ELISA test and compared with a conventional detection method.

Implementation into an ELISA test: optimization and assessment of the sensitivity

After demonstrating the effectiveness of this method using HRP in solution, it was important to investigate the reactivity of this enzyme when acting as a label. In most ELISA tests, HRP is not directly bound to the Ab, but conjugated to streptavidin protein (SA), ready to bind to a biotinylated Ab. This particular process provides consistent measurement of biotinylated detection Ab in sandwich ELISA applications. Thus, a first step consisted in evaluating the enzymatic activity of SA-HRP conjugate in solution (meaning not yet immobilized like in sandwich ELISA conditions) for the developed assay and verify if the optimized conditions are still the more suitable. Surprisingly, with the previous optimal conditions, the TR emission of NPs was 10 times weaker with SA-HRP (Figure S12). After further investigations, it has been found that the only optimized parameter that was not optimal anymore with SA-HRP was the pH of enzymatic reaction, as it was determined to be 7.0 and not 4.6 as for HRP (Figure S13). This can be related to the type of HRP enzyme as mentioned above. Additionally, at pH 7.0, the emission intensity obtained previously with HRP is only recovered when using 10 mmol·L^{-1} succinate (the same buffer used at pH 4.6, although pH 7.0 is out of its buffer range) instead of an appropriate buffer for this pH such as HEPES or TRIS buffer (Figure S14). Thus, the nature of buffer appears to be another factor for the enzymatic reaction. For the following experiments, it was decided to keep pH 7.0 as a new optimal pH for SA-HRP enzymatic reaction, and to do the enzymatic reaction in succinate 10 mmol·L^{-1} as pH was shown to be unchanged during the course of the reaction. The second step was then to implement this new detection method in an ELISA test. A commercial sandwich ELISA assay for insulin detection was chosen with a colorimetric detection using HRP and TMB as substrate. In this test, the analyte is fixed on a surface immobilized primary antibody (Scheme 1, step 1), then a biotin-functionalized secondary antibody is fixed to the antigen and in a third step, the HRP-streptavidin is added to obtain a HRP conjugated antibody (Scheme 1, step 2).

It is worth noting that these first three steps are the ones described in the protocol of the commercial kit, and each step is separated by a washing step to remove the unfixed

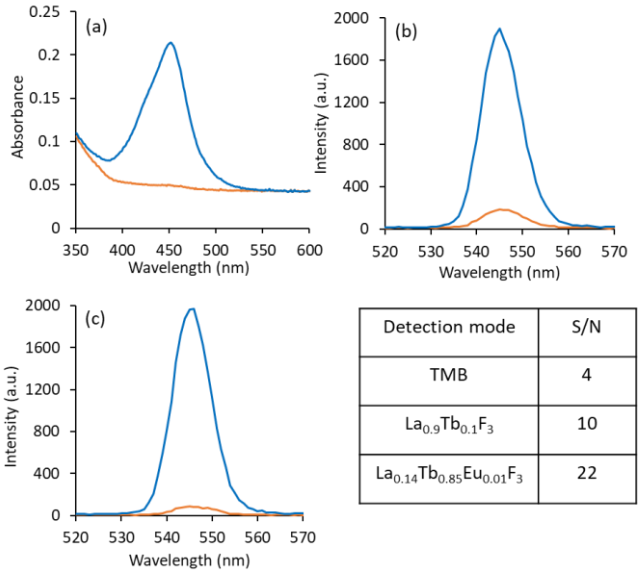

Detection mode	S/N
TMB	4
$La_{0.9}Tb_{0.1}F_3$	10
$La_{0.14}Tb_{0.85}Eu_{0.01}F_3$	22

Figure 9: Absorption spectra of TMB (a) and TR-emission spectra (λ_{exc} = 320 nm) of $La_{0.9}Tb_{0.1}F_3$ NPs (b) and $La_{0.14}Tb_{0.85}Eu_{0.01}F_3$ NPs (c) following an ELISA with 0 (orange) or 20 µU·mL^{-1} (blue) of insulin. Signal over noise response (S/N) is given for each condition in the inset table, calculated from the maximal intensities (450 nm for TMB and 545 nm for NPs).

bio-molecules. As a last step, for the classical ELISA test, a solution containing TMB and H_2O_2 is added, agitated for 15 min and the absorbance at 450 nm is measured after adding an acidic solution to stop the reaction. For our method, a solution containing MHPA and H_2O_2 in succinate is added and incubated under agitation for 1 hour prior to add catalase and the NPs and increase the pH to 13 for TR photoluminescence measurement. For an insulin concentration of 20 µU·mL^{-1}, a signal over noise (S/N) of 4 is obtained with TMB detection while a S/N of 10 is reached with the detection by the MHPA/ $La_{0.9}Tb_{0.1}F_3$ NPs system (Figures 9a and 9b). Moreover, replacing the latter NPs by $Tb_{0.85}La_{0.14}Eu_{0.01}F_3$ NPs led to a two-fold increase of S/N (Figure 9c) originating from the lower background noise.

It is worth noting that initially, $Tb_{0.85}La_{0.14}Eu_{0.01}F_3$ NPs were tested with the expectation of an energy transfer occurring from the Tb to the Eu in the NPs as it has already been reported,[36,37] which would have shifted the emission bands to the red part of the spectrum and would have made two possible channels for the reading of the signal. Unfortunately, this phenomenon could not be observed under our conditions, as evidenced in Figure S15 in the presence of the ligands. In absence of ligand, excitation at 320 nm resulted in a lower signal for Tb at 545 nm that is probably related to the observation of Eu emission due to direct excitation into the $^5H_{4\text{-}6}$ bands of Eu.[38] Thus, despite the absence of the expected energy transfer, the use of $Tb_{0.85}La_{0.14}Eu_{0.01}F_3$ NPs leads to a more sensitive developed detection method.

In a final step, the performance of the developed ELISA was evaluated by establishing the corresponding calibration curve. The assay was performed on a 1-100 µU·mL^{-1} range of insulin concentration under the same optimized conditions mentioned above. $Tb_{0.85}La_{0.14}Eu_{0.01}F_3$ NPs were used in this study for providing the best S/N in the assay. The resulting calibration curve describing the intensity of TR-emission of Tb at 545 nm

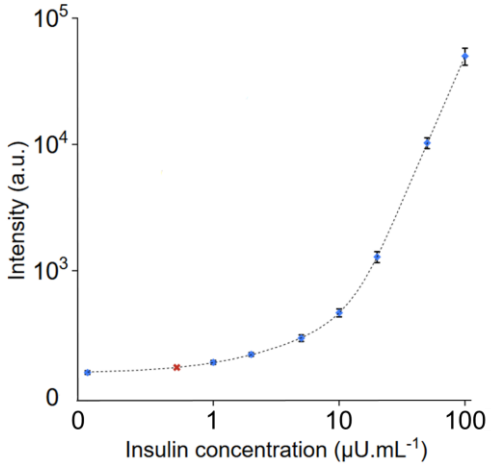

Figure 10: Calibration curve of the photoluminescence response of the assay as a function of insulin concentration (λ_{exc} = 320 nm, λ_{em} = 545 nm). Red dot corresponds to LOD.

after an excitation at 320 nm is shown in Figure 10. The relative response of the assay as a function of the enzyme concentration was fitted in a Spline curve using Assayfit Pro, an ELISA results data analysis software.[39] Spline is a function defined piecewise by polynomials, allowing the fitting of complex smooth shapes. The 3 replicates show weak standard deviations which indicates a good precision of the method. In this range of insulin concentration, the calibration presented a low response curve shape.[40] Most importantly, a LOD of 0.5 µU·mL^{-1} and a LOQ of 1.5 µU·mL^{-1} were determined, corresponding to 3 and 9 pmol·L^{-1} of insulin respectively,[41,42] i.e. a 30 times decrease compared to the LOD/LOQ of in solution free HRP in the best conditions (calibration curve in Figure 8). This sensitivity loss can be attributed to different factors: (i) the nature of HRP enzyme as discussed previously, (ii) the immobilization of the Ab-Antigen-Ab-enzyme complex in the well, the enzymatic reaction being limited by the substrate diffusion rate in solution [43] and (iii) the risk of antigen or SA-HRP loss at each washing step, leading to a overestimation of the real final enzyme concentration in the well.

In parallel, the LOD of the assay using the commercial colorimetric detection was evaluated and determined at 1 µU·mL^{-1}, matching with the LOD provided by the supplier. Thus, despite the sensitivity loss by the method implementation into the ELISA, these results confirmed that with the developed method based on a time resolved detection of Ln NPs photoluminescence, the sensitivity of an ELISA for the quantification of human insulin was improved by a factor of 2.

The reproducibly of the method has also been assessed by realizing the new ELISA test at a given insulin concentration on different days and by changing the batch of insulin kit and measurement parameters, with an obtained S/N average of 20.1 ± 2.3 at 20 µU·mL^{-1} insulin (Table S2).

CONCLUSION

From a systematic study of the HRP catalyzed oxidation of 12 different phenol derivatives by hydrogen peroxide and of the capacity of the oxidation product to efficiently photosensitize Tb doped LaF_3 NPs, MHPA was selected as the most promising substrate for both the enzymatic reaction and the Tb photosensitization. The various parameters influencing the enzymatic re-

action (reaction time, concentration of the reactants, buffer nature, pH) and the Tb photosensitization by the oxidation product (remaining H_2O_2 elimination, NP concentration and type, pH) were carefully optimized to obtain the best conditions leading to the highest TR emission intensity of Tb at a given HRP concentration. It is worth noting that the HRP nature (type and commercial preparation)[29,30] is also an important factor to take into account as very different results were obtained for free HRP initially employed and HRP-SA conjugate from the commercial ELISA kit, requiring further optimization (the most dramatic parameter being the optimal pH for the enzymatic reaction). In solution, enzymatic reaction using $La_{0.9}Tb_{0.1}F_3$ NPs led to a LOD of 0.1 pmol·L^{-1} for free HRP, 8000 and 20 times more sensitive than the best conditions of similar detection methods with Ln complexes,[25,35] with a calibration curve covering three orders of magnitude and an unreached upper limit of linearity, highlighting a large dynamic concentration range for HRP quantification. Finally, the implementation of this detection method into commercially available sandwich ELISA assay for human insulin quantification was successfully accomplished with $La_{0.14}Tb_{0.85}Eu_{0.1}F_3$ NPs, with atwo times higher sensitivity compared to colorimetric TMB detection method of the commercial kit. Moreover, this proof-of-concept was realized with human insulin but this detection method could be implemented on any HRP-based ELISA assay, with the same gain of sensitivity compared with TMB tests, as it is independent of the nature of the antigen/antibody system. As a perspective, a moderately increased temperature and sequential addition of small amounts of H_2O_2 were reported to enhance the yield of phenol dimerization.[44,45] These procedures were practically unfeasible in our laboratory, however with an automatized assay and using injectors for the different addition steps, these are serious options to improve the response of the assay.

ASSOCIATED CONTENT

Supporting Information

The Supporting Information is available free of charge on the ACS Publications website.

Preparation of the $La_{0.14}Tb_{0.85}Eu_{0.1}F_3$ nanoparticles; Procedure of synthesis of the MHPA dimer; Hydrodynamic diameter of NPs; Mobility of NPs; XRD pattern of NPs; elemental mass concentrations of Ln by ICP-AES; TR emission spectra of NPs with various substrates without HRP; TR emission spectra of NPs with addition of various quantities of NaOH solution; TR emission spectra of NPs with various substrates after enzymatic reaction; Chromatogram of the reaction mixture with and without HRP; Chromatogram of reaction mixture with different additions of H_2O_2; Excitation and emission spectra of MHPA related dimer; Fluorescence intensity of dimer as a function of substrate concentration; Calibration curve of the photoluminescence response of the assay as a function of HRP concentration; TR emission spectra of NPs after MHPA oxidation by HRP or SA-HRP; Fluorescence intensity of MHPA dimer as a function of reaction pH; TR emission spectra of NPs after MHPA oxidation in different buffers; TR emission spectra of $La_{0.14}Tb_{0.85}Eu_{0.01}F_3$ NPs and $La_{0.9}Tb_{0.1}F_3$ NPs after MHPA oxidation by SA-HRP; Reproducibility measurement at a given insulin concentration.

AUTHOR INFORMATION

Corresponding Author

* Dr. Loïc J. Charbonnière, l.charbonn@unistra.fr

Present Addresses

† Univ Strasbourg, Lab Bioimagerie & Pathol, Fac Pharm, CNRS UMR 7021, CS60024 74,Route Rhin, F-67401 Illkirch Graffenstaden, France

Author Contributions

The manuscript was written through contributions of all authors. All authors have given approval to the final version of the manuscript.

ACKNOWLEDGMENT

This work was supported by the French National Research Agency through “Programme d’investissement d’Avenir” under contrat ANR-17-EURE-0024. The “Plateforme Analytique des Inorganiques” (unistra) is acknowledged for the ICP-AES measurements. The authors thank Lai Truong Phuoc for the XRD analysis of $La_{0.14}Tb_{0.85}Eu_{0.1}F_3$ NPs.

REFERENCES

(1) Utochnikova, V. V. Chapter 318 - Lanthanide Complexes as OLED Emitters. In *Handbook on the Physics and Chemistry of Rare Earths*; Bünzli, J.-C. G., Pecharsky, V. K., Eds.; Including Actinides; Elsevier, 2021; Vol. 59, pp 1–91. https://doi.org/10.1016/bs.hpcre.2021.05.001.

(2) Gavriluta, A.; Fix, T.; Nonat, A.; Slaoui, A.; Guillemoles, J.-F.; Charbonnière, L. J. Tuning the Chemical Properties of Europium Complexes as Downshifting Agents for Copper Indium Gallium Selenide Solar Cells. *J. Mater. Chem. A* **2017**, *5* (27), 14031–14040. https://doi.org/10.1039/C7TA02892J.

(3) Kitagawa, Y.; Nakai, T.; Hosoya, S.; Shoji, S.; Hasegawa, Y. Luminescent Lanthanide Complexes for Effective Oxygen-Sensing and Singlet Oxygen Generation. *ChemPlusChem* **2023**, *88* (6), e202300149. https://doi.org/10.1002/cplu.202300149.

(4) Sy, M.; Nonat, A.; Hildebrandt, N.; Charbonnière, L. J. Lanthanide-Based Luminescence Biolabelling. *Chem. Commun.* **2016**, *52* (29), 5080–5095. https://doi.org/10.1039/C6CC00922K.

(5) Amoroso, A. J.; Pope, S. J. A. Using Lanthanide Ions in Molecular Bioimaging. *Chem. Soc. Rev.* **2015**, *44* (14), 4723–4742. https://doi.org/10.1039/C4CS00293H.

(6) Bünzli, J.-C. G.; Piguet, C. Taking Advantage of Luminescent Lanthanide Ions. *Chem. Soc. Rev.* **2005**, *34* (12), 1048–1077. https://doi.org/10.1039/B406082M.

(7) Liu, Y.; Tu, D.; Zhu, H.; Chen, X. Lanthanide-Doped Luminescent Nanoprobes: Controlled Synthesis, Optical Spectroscopy, and Bioapplications. *Chem. Soc. Rev.* **2013**, *42* (16), 6924–6958. https://doi.org/10.1039/C3CS60060B.

(8) Bao, G.; Wen, S.; Lin, G.; Yuan, J.; Lin, J.; Wong, K.-L.; Bünzli, J.-C. G.; Jin, D. Learning from Lanthanide Complexes: The Development of Dye-Lanthanide Nanoparticles and Their Biomedical Applications. *Coord. Chem. Rev.* **2021**, *429*, 213642. https://doi.org/10.1016/j.ccr.2020.213642.

(9) Zhu, X.; Zhang, H.; Zhang, F. Ligand-Based Surface Engineering of Lanthanide Nanoparticles for Bioapplications. *ACS Mater. Lett.* **2022**, *4* (9), 1815–1830. https://doi.org/10.1021/acsmaterialslett.2c00528.

(10) Hemmilá, I.; Mukkala, V.-M. Time-Resolution in Fluorometry Technologies, Labels, and Applications in Bioanalytical Assays. *Crit. Rev. Clin. Lab. Sci.* **2001**, *38* (6), 441–519. https://doi.org/10.1080/20014091084254.

(11) Hildebrandt, N.; Charbonnière, L. J.; Löhmannsröben, H.-G. Time-Resolved Analysis of a Highly Sensitive Förster Resonance Energy Transfer Immunoassay Using Terbium Complexes as Donors and Quantum Dots as Acceptors. *J. Biomed. Biotechnol.* **2007**, *2007*, 79169. https://doi.org/10.1155/2007/79169.

(12) Evangelista, R. A.; Pollak, A.; Gudgin Templeton, E. F. Enzyme-Amplified Lanthanide Luminescence for Enzyme Detection in Bioanalytical Assays. *Anal. Biochem.* **1991**, *197* (1), 213–224. https://doi.org/10.1016/0003-2697(91)90381-3.

(13) Steinkamp, T.; Karst, U. Detection Strategies for Bioassays Based on Luminescent Lanthanide Complexes and Signal Amplification. *Anal. Bioanal. Chem.* **2004**, *380* (1), 24–30. https://doi.org/10.1007/s00216-004-2682-2.

(14) Hagan, A. K.; Zuchner, T. Lanthanide-Based Time-Resolved Luminescence Immunoassays. *Anal. Bioanal. Chem.* **2011**, *400* (9), 2847–2864. https://doi.org/10.1007/s00216-011-5047-7.

(15) Beeby, A.; Clarkson, I. M.; Dickins, R. S.; Faulkner, S.; Parker, D.; Royle, L.; Sousa, A. S. de; Williams, J. A. G.; Woods, M. Non-Radiative Deactivation of the Excited States of Europium, Terbium and Ytterbium Complexes by Proximate Energy-Matched OH, NH and CH Oscillators: An Improved Luminescence Method for Establishing Solution Hydration States. *J. Chem. Soc. Perkin Trans. 2* **1999**, No. 3, 493–504. https://doi.org/10.1039/A808692C.

(16) Charbonnière, L.; Mameri, S.; Kadjane, P.; Platas-Iglesias, C.; Ziessel, R. Tuning the Coordination Sphere around Highly Luminescent Lanthanide Complexes. *Inorg. Chem.* **2008**, *47* (9), 3748–3762. https://doi.org/10.1021/ic702472n.

(17) Cheignon, C.; Kassir, A. A.; Soro, L. K.; Charbonnière, L. J. Dye-Sensitized Lanthanide Containing Nanoparticles for Luminescence Based Applications. *Nanoscale* **2022**, *14* (38), 13915–13949. https://doi.org/10.1039/D1NR06464A.

(18) Goetz, J.; Nonat, A.; Diallo, A.; Sy, M.; Sera, I.; Lecointre, A.; Lefevre, C.; Chan, C. F.; Wong, K.-L.; Charbonnière, L. J. Ultrabright Lanthanide Nanoparticles. *ChemPlusChem* **2016**, *81* (6), 526–534. https://doi.org/10.1002/cplu.201600007.

(19) Cardoso, D. S. M.; Charbonniere, L.; Charpentier, C.; Cifliku, V.; Goetz, J.; Hildebrandt, N.; Nonat, A.; Wong, K.-L. Nanoparticules De Lanthanide Luminescentes Ultra Brillantes Comprenant Du Terbium Et Ayant Une Durée De Vie Plus Longue À L'état Excité. EP3591024A1, January 8, 2020.

(20) Cheignon, C.; Heurté, M.; Knighton, R. C.; Kassir, A. A.; Lecointre, A.; Nonat, A.; Boos, A.; Christine, C.; Asfari, Z.; Charbonnière, L. J. Investigation of the Supramolecular Assembly of Luminescent Lanthanide Nanoparticles Surface Functionalized by P-Sulfonato-Calix[4]Arenes with Charged Aromatic Compounds. *Eur. J. Inorg. Chem.* **2021**, *2021* (36), 3761–3770. https://doi.org/10.1002/ejic.202100546.

(21) Yu, Jian.; Taylor, K. E.; Zou, Huixian.; Biswas, Nihar.; Bewtra, J. K. Phenol Conversion and Dimeric Intermediates in Horseradish Peroxidase-Catalyzed Phenol Removal from Water. *Environ. Sci. Technol.* **1994**, *28* (12), 2154–2160. https://doi.org/10.1021/es00061a025.

(22) Jonsson, M.; Lind, J.; Merényi, G. Redox and Acidity Properties of 2,2'- and 4,4'-Biphenol and the Corresponding Phenoxyl Radicals. *J. Phys. Chem. A* **2002**, *106* (18), 4758–4762. https://doi.org/10.1021/jp0129232.

(23) Guilbault, G. G.; Brignac, P. J.; Juneau, Mark. Substrates for the Fluorometric Determination of Oxidative Enzymes. *Anal. Chem.* **1968**, *40* (8), 1256–1263. https://doi.org/10.1021/ac60264a027.

(24) Guilbault, G. G.; Brignac, P. J.; Zimmer, Mary. Homovanillic Acid as a Fluorometric Substrate for Oxidative Enzymes. Analytical Applications of the Peroxidase, Glucose Oxidase, and Xanthine Oxidase Systems. *Anal. Chem.* **1968**, *40* (1), 190–196. https://doi.org/10.1021/ac60257a002.

(25) Zheng, X.-Y.; Lu, J.-Z.; Zhu, Q.-Z.; Xu, J.-G.; Li, Q.-G. Study of a Lanthanide Fluorescence System With a Coupled Reaction-Based on Hemin Catalysis. *Analyst* **1997**, *122* (5), 455–458. https://doi.org/10.1039/A606560K.

(26) Huang, L.; Colas, C.; Ortiz de Montellano, P. R. Oxidation of Carboxylic Acids by Horseradish Peroxidase Results in Prosthetic Heme Modification and Inactivation. *J. Am. Chem. Soc.* **2004**, *126* (40), 12865–12873. https://doi.org/10.1021/ja046455w.

(27) Manstein, D.; Preller, M.; Furch, M.; Kalesse, M.; Diaz, N. Biphenyl Compounds for Use in Treating Malaria and Other Parasitic Disorders. EP2753599A1, July 16, 2014. https://patents.google.com/patent/EP2753599A1/en (accessed 2023-02-21).

(28) Lopes, G. R.; Pinto, D. C. G. A.; Silva, A. M. S. Horseradish Peroxidase (HRP) as a Tool in Green Chemistry. *RSC Adv.* **2014**, *4* (70), 37244–37265. https://doi.org/10.1039/C4RA06094F.

(29) Floyd, R. A.; Soong, L. M.; Culver, P. L. Horseradish Peroxidase/Hydrogen Peroxide-Catalyzed Oxidation of the Carcinogen N-Hydroxy-N-Acetyl-2-Aminofluorene as Effected by Cyanide and Ascorbate1. *Cancer Res.* **1976**, *36* (4), 1510–1519.

(30) Krainer, F.; Naeaetsaari, L.; Glieder, A.; Kulterer, M.; Reichel, V. Horseradish Peroxidase Isoenzymes. US20140363837A1, December 11, 2014. https://patents.google.com/patent/US20140363837A1/en (accessed 2022-10-12).

(31) Veitch, N. C. Horseradish Peroxidase: A Modern View of a Classic Enzyme. *Phytochemistry* **2004**, *65* (3), 249–259. https://doi.org/10.1016/j.phytochem.2003.10.022.

(32) Hiner, A. N. P.; Hernández-Ruíz, J.; Arnao, M. B.; García-Cánovas, F.; Acosta, M. A Comparative Study of the Purity, Enzyme Activity, and Inactivation by Hydrogen Peroxide of Commercially Available Horseradish Peroxidase Isoenzymes A and C. *Biotechnol. Bioeng.* **1996**, *50* (6), 655–662. https://doi.org/10.1002/(SICI)1097-0290(19960620)50:6<655::AID-BIT6>3.0.CO;2-J.

(33) Chen, S. X.; Schopfer, P. Hydroxyl-Radical Production in Physiological Reactions. A Novel Function of Peroxidase. *Eur. J. Biochem.* **1999**, *260* (3), 726–735. https://doi.org/10.1046/j.1432-1327.1999.00199.x.

(34) Hoshino, N.; Nakajima, R.; Yamazaki, I. The Effect of Polymerization of Horseradish Peroxidase on the Peroxidase Activity in the Presence of Excess H_2O_2: A Background for a Homogeneous Enzyme Immunoassay. *J. Biochem. (Tokyo)* **1987**, *102* (4), 785–791. https://doi.org/10.1093/oxfordjournals.jbchem.a122116.

(35) Meyer, J.; Karst, U. Peroxidase Enhanced Lanthanide Luminescence—a New Technique for the Evaluation of Bioassays. *Analyst* **2000**, *125* (9), 1537–1538. https://doi.org/10.1039/B004973P.

(36) Nonat, A.; Liu, T.; Jeannin, O.; Camerel, F.; Charbonnière, L. J. Energy Transfer in Supramolecular Heteronuclear Lanthanide Dimers and Application to Fluoride Sensing in Water. *Chem. – Eur. J.* **2018**, *24* (15), 3784–3792. https://doi.org/10.1002/chem.201705532.

(37) Yang, W.; Zhang, Z.; Zhang, T.; Zhang, X.; Shi, X.; Li, C.; Wang, X.; Leng, Z.; Jiang, X.; Liu, H.; Li, Y.; Li, S.; Lin, H.; Huang, K.; Zeng, F.; Li, C.; Su, Z. White Light Emission and Fluorescence Enhancement of Rare Earth RE^{3+} (Tb, Eu, Dy) Doped CeF_3 Nanoparticles. *J. Lumin.* **2022**, *242*, 118535. https://doi.org/10.1016/j.jlumin.2021.118535.

(38) Binnemans, K. Interpretation of Europium(III) Spectra. *Coord. Chem. Rev.* **2015**, *295*, 1–45. https://doi.org/10.1016/j.ccr.2015.02.015.

(39) Curve Fitting for Laboratory Assays - AssayFit Pro. https://www.assayfit.com (accessed 2022-10-28).

(40) Davis, D.; Zhang, A.; Etienne, C.; Huang, I.; Malit, M. *Principles of curve fitting for multiplex sandwich immunoassays*. Bio-Rad Laboratories, Inc. Alfred Nobel Drive, Hercules, CA.

(41) Knopp, J. L.; Holder-Pearson, L.; Chase, J. G. Insulin Units and Conversion Factors: A Story of Truth, Boots, and Faster Half-Truths. *J. Diabetes Sci. Technol.* **2018**, *13* (3), 597–600. https://doi.org/10.1177/1932296818805074.

(42) Bristow, A. F.; Das, R. E.; Bangham, D. R. World Health Organization International Standards for Highly Purified Human, Porcine and Bovine Insulins. *J. Biol. Stand.* **1988**, *16* (3), 165–178. https://doi.org/10.1016/0092-1157(88)90004-2.

(43) Khan, M. R. Immobilized Enzymes: A Comprehensive Review. *Bull. Natl. Res. Cent.* **2021**, *45* (1), 207. https://doi.org/10.1186/s42269-021-00649-0.

(44) Akita, M.; Tsutsumi, D.; Kobayashi, M.; Kise, H. Structural Change and Catalytic Activity of Horseradish Peroxidase in Oxidative Polymerization of Phenol. *Biosci. Biotechnol. Biochem.* **2001**, *65* (7), 1581–1588. https://doi.org/10.1271/bbb.65.1581.

(45) Wu, J.; Bewtra, J. K.; Biswas, N.; Taylor, K. E. Effect of H_2O_2 Addition Mode on Enzymatic Removal of Phenol from Wastewater in the Presence of Polyethylene Glycol. *Can. J. Chem. Eng.* **1994**, *72* (5), 881–886. https://doi.org/10.1002/cjce.5450720515.

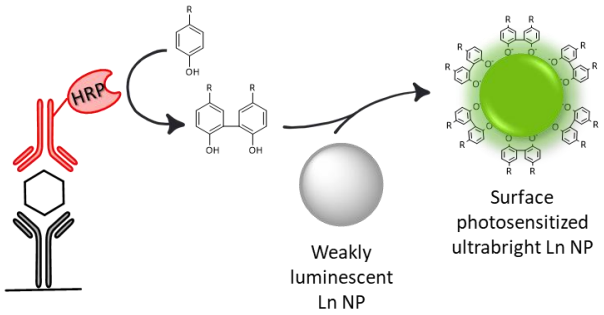
HRP
Weakly luminescent Ln NP
Surface photosensitized ultrabright Ln NP